Determination of atomic positions and polar direction in half-Heusler material $Sb_{1-x}Sn_xTi_{1-y-z}Hf_yZr_zCo$ using electron channeling

Cite as: AIP Advances **8**, 125335 (2018); https://doi.org/10.1063/1.5042816
Submitted: 05 June 2018 . Accepted: 18 December 2018 . Published Online: 31 December 2018

Vidar Hansen, Cristina Echevarria-Bonet, Mona Wetrhus Minde, and Johan Taftø

Determination of atomic positions and polar direction in half-Heusler material $Sb_{1-x}Sn_xTi_{1-y-z}Hf_yZr_zCo$ using electron channeling

Vidar Hansen,[1] Cristina Echevarria-Bonet,[2,a] Mona Wetrhus Minde,[1,b] and Johan Taftø[3]

[1]*Department of Mechanical and Structural Engineering and Materials Science, University of Stavanger, N-4036 Stavanger, Norway*
[2]*Physics Department, Institute of Energy Technology, P.O. Box 40, N-2027 Kjeller, Norway*
[3]*Department of Physics, Centre for Materials Science and Nanotechnology, University of Oslo, P.O. Box 1048 Blindern, N-0316 Oslo, Norway*

(Received 5 June 2018; accepted 18 December 2018; published online 31 December 2018)

Variation of electron-induced x-ray emission with the crystal direction of an incoming electron beam (channeling) is used to study the crystal site preference of different elements in a promising thermoelectric half-Heusler material. This material has Sb, Co and Ti as the main constituting elements, with lower contents of Hf, Zr and Sn. It is confirmed experimentally, in accordance with previous assumptions, that Sb and Sn occupy one of the octahedral sites, 4a (0, 0, 0), Ti, Zr and Hf the other octahedral site, 4b (½, ½, ½), and Co atoms occupy the tetrahedral site, 4c (¼, ¼, ¼) in the cubic spacegroup F$\bar{4}$3m with lattice constant a = 0.598 ± 0.001 nm. Furthermore, a strong asymmetry along the polar directions is observed, which is as it should be in a half-Heusler material, when the Co atoms have a strong preference for one of the two sets of tetrahedral sites. Such asymmetries can not be observed by kinematical diffraction according to Friedel's law, thus demonstrating that the observation of element characteristic signals under channeling conditions is a unique technique for determining the sense of polar directions and distinguishing crystal symmetry alternatives in small crystal grains and nanocrystals. https://doi.org/10.1063/1.5042816

I. INTRODUCTION

The search for materials with low thermal conductivity is an important issue within several fields of materials science. Examples of such materials are thermoelectric materials where atomic disorder may contribute to reduced thermal conductivity, which may result in higher energy efficiency of the materials used in thermoelectric heat pumps and electricity generators. To better understand the lattice (phonon) contribution to thermal conductivity,[1] the crystal site preference for the different elements and the spatial variations in compositions are useful information. In this study, variation in electron-induced element characteristic x-ray emission under electron channeling conditions[2] is used to address site occupancy on the three different crystal sites for the six elements in the half-Heusler material $Sb_{1-x}Sn_xTi_{1-y-z}Hf_yZr_zCo$. For certain x, y and z values, this material is an excellent p-type thermoelectric material.[3,4] Particular attention is given to the practical use of this electron channeling technique (also referred to as ALCHEMI[5]) to determine the site preferences as well as to addressing the lack of inversion symmetry in half-Heusler materials.

[a]Present address: Department of Physics, University of Oviedo, E-33007 Oviedo, Spain
[b]Corresponding author: mona.w.minde@uis.no

II. SPECIMEN PREPARATION AND ELECTRON MICROSCOPE EQUIPMENT

The material was fabricated by arc-melting powders of the different elements in the stoichiometric proportions expressed by the chemical formula $Sb_{0.8}Sn_{0.2}Ti_{0.5}Hf_{0.25}Zr_{0.25}Co$, with subsequent ball milling followed by spark plasma sintering. Figure 1 shows an electron-induced x-ray emission spectrum obtained using a scanning electron microscope (SEM) equipped with an energy-dispersive x-ray spectrometer (EDAX). Table I shows the compositions in different regions as determined from the x-ray spectra. Figure 2a shows an SEM image obtained by detecting backscattered electrons, and Figs. 2b–g show SEM images obtained by mapping using characteristic x-rays emission from the six different elements. The inhomogeneities in Ti, Zr and Hf contents are similar to those observed in other half-Heusler thermoelectric materials.[6,7]

Crushed fragments of the material were used for the channeling studies in a JEOL 2100 transmission electron microscope with a LaB_6 electron source, operating at 200 kV. The x-ray emission spectra under electron channeling conditions were collected with an energy-dispersive spectrometer, also of EDAX type.

III. CHANNELING TECHNIQUE

Electron channeling experiments to obtain crystallographic information from the electron-induced x-ray emission were performed with a convergent beam of electrons focused on the specimen.[8] In planar channeling experiments, all reflections should be avoided except those along a certain reciprocal lattice row. A well-defined crystal orientation is required for these experiments. Thus, a convergent beam, focused on a small, thin area of diameter around 10 nm, is necessary because a crystal of thickness below half an extinction length, typically below 50 nm, is needed. If a parallel beam is used, a larger thin area needs to be illuminated to obtain enough x-ray counts. However, a large thin area tends to bend, resulting in variation of the crystal orientation over the illuminated

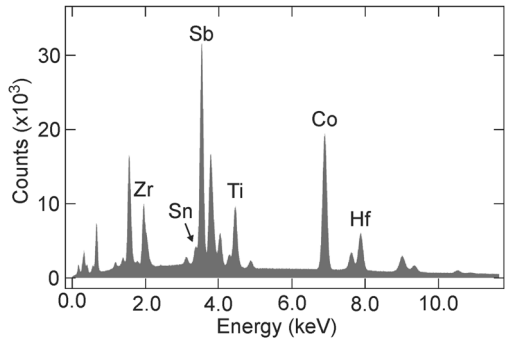

FIG. 1. X-ray emission spectrum collected using an SEM. X-ray emission lines used for the mapping in Fig. 2 are marked with their respective element.

TABLE I. Compositions in different regions determined from SEM x-ray emission spectra, given in atom percent. EDS quantifications are performed with ZAF corrections without the use of standard. The errors for all elements are less than 1%.

Sb	30.0	28.6	30.3	29.7	23.8	16.9	28.3
Sn	2.7	3.6	2.6	2.7	8.1	13.7	4.3
Co	36.7	36.6	36.0	36.7	36.9	38.4	35.3
Ti	9.7	15.1	10.3	10.0	21.1	22.4	15.2
Zr	8.3	6.7	8.7	8.2	4.7	4.6	7.5
Hf	12.6	9.4	12.1	12.7	5.4	4.0	9.4
Sb + Sn	32.7	32.2	32.9	32.4	31.9	30.6	32.6
Co	36.7	36.6	36.0	36.7	36.9	38.4	35.3
Ti + Zr + Hf	30.6	31.2	31.1	30.9	31.2	31.0	32.1
Sum	**100.0**	**100.0**	**100.0**	**100.0**	**100.0**	**100.0**	**100.0**

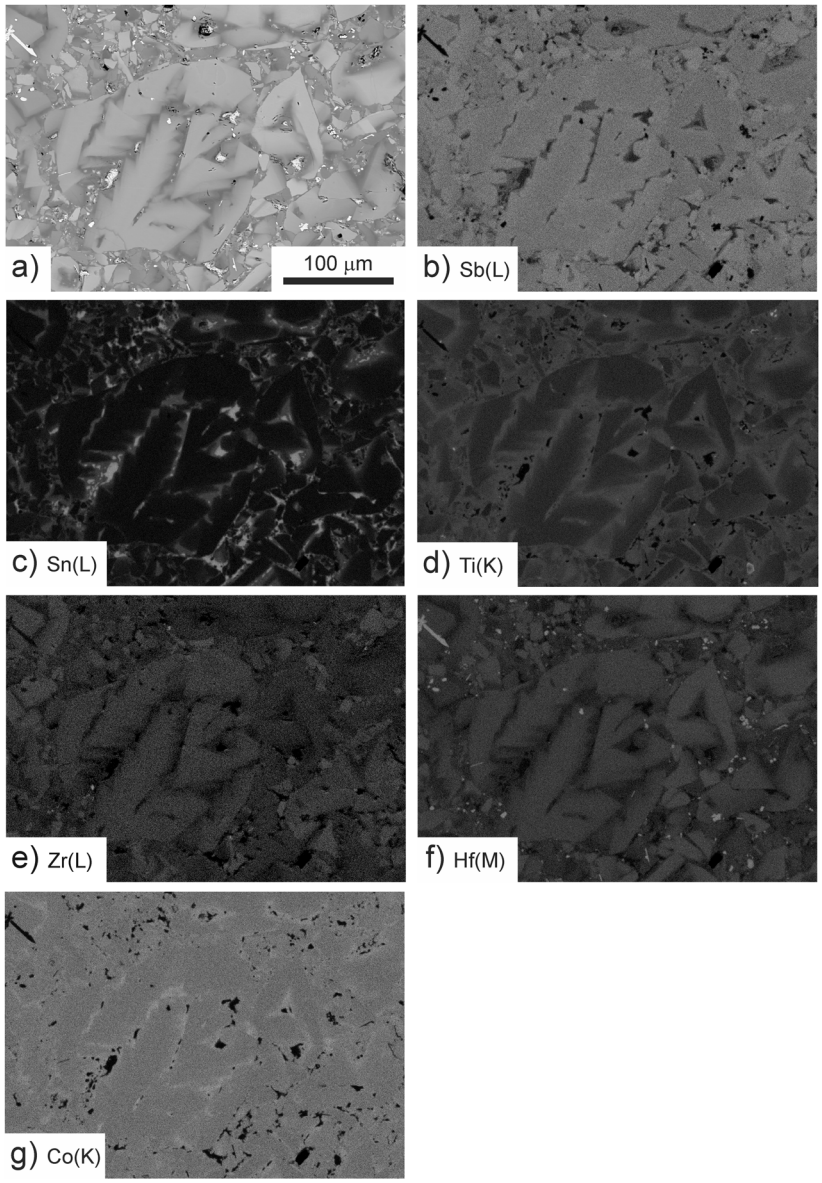

FIG. 2. SEM images, all from the same area: a) using backscattered electrons, and b)–g) showing the distribution of the elements mapped using element characteristic x-ray signals from Sb, Sn, Ti, Zr, Hf and Co, respectively, see Fig. 1. Bright areas represent heavy atoms in a) and high x-ray emission in b)–g). g) and b) show dark areas that are bright in c) suggesting areas with very high Sn concentration. Similarly, bright regions in g) correlate with bright regions in c), suggesting a phase with high content of Co and Sn. These phases were avoided in the channeling measurements.

area, and thus lack of control of the exact crystal orientation. Introductory experiments, in line with previous experience, confirmed that a convergent beam is favorable. The convergence of the electron beam should be small enough to avoid overlap between the diffraction disks, and the electron probe on the specimen so small as to cover only a thin area at the edge of the specimen. The convergence angle was in this study around 1.5 mrad.

For brittle materials, a good way of preparing the specimen is by grinding small pieces of the material submerged in ethanol in a mortar. A drop of the mixture of ethanol and the tiny fragments of material are then placed on a holey carbon film. (Ion milling may produce a relatively large volume fraction of disordered or amorphous material on the thin areas of the crystal foil.)

Let us now look specifically at procedures to obtain information about the site occupancy by noting that channeling causes modulation of the electron wave field within the crystal unit cell.[2,8] Figure 3 shows the half-Heusler structure projected down the [010] and [1$\bar{1}$0] directions together with a sequence of atomic planes along the directions [100], [110], [111] and [$\bar{1}\bar{1}$3].

Note that in Fig. 3, along the [110] direction, all atom planes contain C, N and T sites, and thus have the same composition as the whole crystal. On the other hand, across the (100) plane, there are alternating planes with different crystal sites. Two of the three sites in a half-Heusler material are on one of the planes and one site is on the plane halfway in between. As an analogy to the NaCl structure, the plane with two sites is referred to as the plane with octahedral C sites, 4a (0, 0, 0), and octahedral N sites, 4b (½, ½, ½), and the plane in between with one site as the T site, 4c (¼, ¼, ¼), (T stands for the tetrahedral position in the NaCl structure). Across the (111) and ($\bar{1}\bar{1}$3) planes, it can be seen that there are three separate planes, one containing the C sites, one containing the N sites and one containing the T sites. Furthermore, there is a lack of inversion symmetry across the (111) and ($\bar{1}\bar{1}$3) planes.

As an alternative to relying on drawings of the projected structure to find useful conditions for performing channeling experiments, an expression for the structure factors[8] can be considered. This is particularly convenient for more complicated structures. For the half-Heusler materials, there are three types of reflections:

$$\text{Reflections with h + k + l = 4n such as (220), (400), etc., where } F_{hkl} = 4(f_C + f_N + f_T) \tag{1}$$

$$\text{Reflections with h + k + l = 4n + 2 such as (200), (222), etc., where } F_{hkl} = 4(f_C + f_N - f_T) \tag{2}$$

Reflections with h, k and l all odd numbers give two alternatives as a consequence of the lack of inversion symmetry:

$$F_{hkl} = 4(f_C - f_N + f_T \exp i\left(2\pi n + \frac{\pi}{2}\right)) \text{ or } F_{hkl} = 4(f_C - f_N + f_T \exp i\left(2\pi n + \frac{3\pi}{2}\right)) \tag{3}$$

The sequence of planes in Fig. 3 can be expressed as phase factors for the different crystal sites. For example, Eq. (2) shows that the scattering from atoms at the T site is π out of phase (negative sign in front of f_T) with the scattering of atoms at the C and N sites.

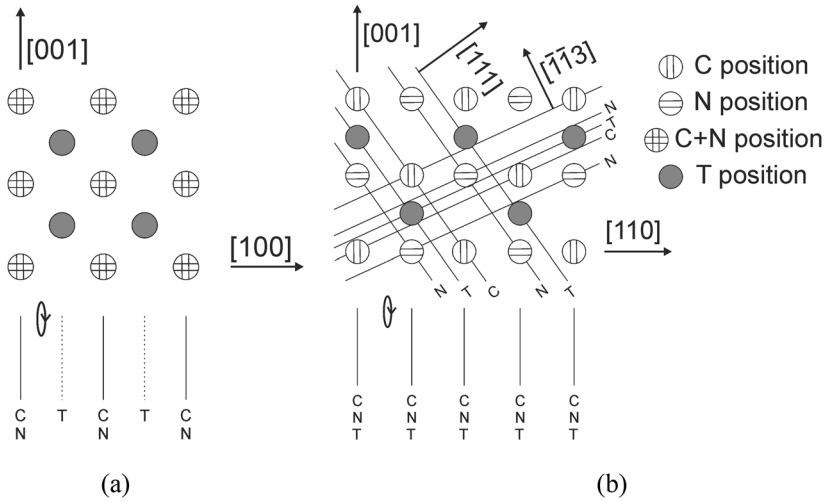

FIG. 3. Projected structure of a half-Heusler material along the [010] direction and the [1$\bar{1}$0] direction with sequences of planes along the [100], [110], [111] and [$\bar{1}\bar{1}$3] directions. The illustrated sequences of planes are those encountered in planar channeling by tilting around the appropriate axis away from the [010] and [1$\bar{1}$0] projections.

IV. EXPERIMENTAL RESULTS

Typical compositions of the TEM samples were as measured by the SEM, Table I. Figure 4 shows normalized x-ray emission as a function of angle between the incident beam and the lattice planes. Here, the incident beam forms small angles with the (100) planes in Fig. 4a, and with the (111) planes in Fig. 4b. The error (meaning a combination of random and systematic error) for the different elements are indicated in the front of the element symbol.

Note the symmetry around the (100) planes and the deviation from symmetry around the (111) planes, which is in agreement with what is the case in a half-Heusler material as seen in Fig. 3. Table II presents measurements of the ratio between the normalized x-ray emission for five pairs of spectra with the 311 and $\bar{3}\bar{1}\bar{1}$ reflections at the Bragg position.

For the elements Sb and Sn, this ratio is consistently below unity, and for Ti, Zr and Hf above unity, demonstrating that this channeling technique is highly sensitive to lack of inversion symmetry. For Co this ratio is close to unity because the Co atoms are located close to the position where the sine curve in Fig. 8. crosses from below to above 1.0.

After having established the symmetry for the 100-reciprocal row, Fig. 4a, more careful measurements are performed on one half of the row, Fig. 5. This is done with longer acquisition time on a thinner area exhibiting stronger channeling effect. There is thus better counting statistics, so the uncertainty is reduced. (Note for example the larger variation in the normalized x-ray counts for Co in Fig. 5 than in Fig. 4a.) The focus in Fig. 4a is the symmetry across the 100 reciprocal row. In Fig. 5 the elements Sb, Sn, Ti, Zr and Hf follow the same curve, indicating small errors. Only two of the 32 points deviate noticeably from this curve.

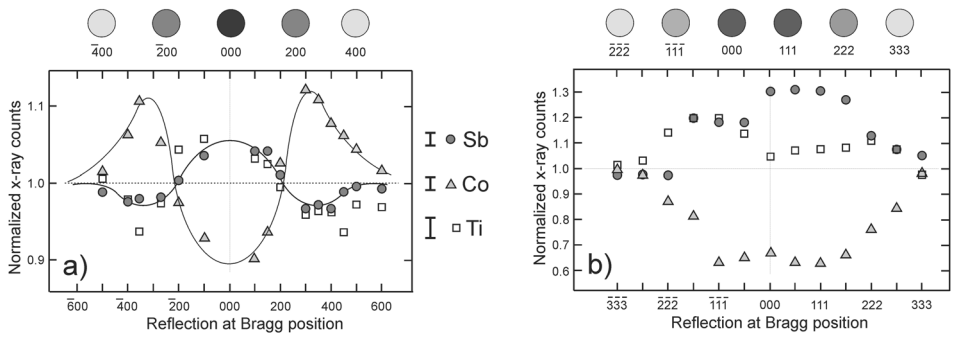

FIG. 4. Normalized x-ray yield for 15 incident beam directions in a) and 13 directions in b). a) 100-reciprocal lattice row. For clarity curves are drawn only for the two majority elements with the best counting statistics, Co and Sb. The fluctuations for Ti are much larger because of poorer counting statistics and disturbance due to concentration variations associated with phase separation. b) 111-reciprocal lattice row shows lack of symmetry, in particularly for Sb and Ti. Typical diffraction patterns are indicated above with the beam parallel to the atomic planes in a, and the Bragg position fulfilled for the 111 reflection in b.

TABLE II. Ratio between normalized x-ray emission counts with the 311 and $\bar{3}\bar{1}\bar{1}$ reflection at the Bragg positions for five pairs of measurements. The lower row shows the weighted average for the minority elements Hf and Zr, and Ti involved in the phase separation.

Measurement	1	2	3	4	5	Average
Sb	0.85	0.81	0.87	0.92	0.88	0.87
Sn	0.85	0.75	0.85	0.86	0.82	0.83
Co	1.00	0.98	1.00	0.91	1.02	0.98
Ti	1.15	1.14	1.07	1.04	1.11	1.10
Zr	1.33	1.31	1.31	1.12	1.13	1.23
Hf	1.11	1.13	1.20	1.48	1.07	1.18
Ti + Zr + Hf	1.19	1.15	1.16	1.17	1.11	1.16

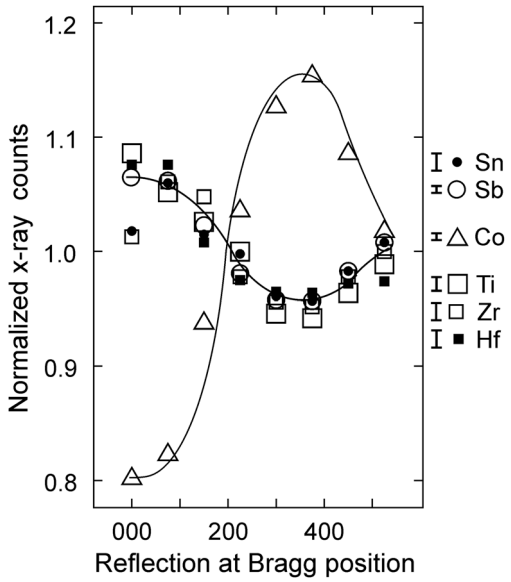

FIG. 5. Variation in x-ray emission along the 100-reciprocal row for the six elements for a longer acquisition time and thus better counting statistics than in Fig. 4. As a guide, curves are drawn for the main elements Co and Sb. Apart from two exceptions, the 32 points for Sn, Ti, Zr and Hf follow the curve of Sb closely. The error bars for the different elements are indicated in front of the element symbols.

V. DISCUSSION

Qualitatively, the observations are intuitively explained by classical physics considerations, while wave mechanical calculations (for example Bloch wave calculations) are used for more quantitative studies. At the atomic planes, the incident electrons see wells in the Coulomb potential and are thus attracted to the atoms if they enter parallel to the planes, and more so to the deep wells caused by the presence of elements with high atomic numbers. The uppermost part of the atomic planes may be looked upon as cylindrical lenses that focus the electrons as illustrated in Fig. 6. If the beam is slightly tilted, the intensity of the wave field tends to be on one side of the planes for a very thin crystal. If the crystal lacks inversion symmetry across a plane, there may be an asymmetry in the x-ray yield for the same amount of tilting in opposite directions relative to the lattice planes. The reason for this asymmetry is that the x-ray yield is proportional to the electron wave-field intensity at the atom. This was observed for the (111) planes in Fig. 4b and for the (311) planes in Table II.

Many beam Bloch wave calculations are useful for more detailed study of the electron wave field within the crystal for a given thickness and direction of incident beam. However, it is a challenge to accurately determine the experimental conditions in terms of thickness and crystal orientation for the small crystal volumes and the small tilts of the incident beam in this work.

Figure 7 shows qualitative two-beam Bloch wave calculations of the thickness-integrated wave-field modulations for thin crystals for three incident beam directions.

Exactly at the Bragg position, where the two Bloch waves are equally excited, there is a uniform wave-field intensity over the crystal unit cell. However, for crystals of thickness well below an extinction length, the thickness-integrated wave field exhibits a considerable variation across the unit cell. Disregarding what is often referred to as absorption, which is diffuse scattering out of the incident and Bragg reflected beams, the wave field at thickness z and position x within the repetition unit is given by[9]

$$I(x,z) = 1 - \sin(2\pi g x)\sin(2\pi(\gamma_1 - \gamma_2)z) \tag{4}$$

This equation is based on two-beam Bloch wave calculations. Here $(\gamma_1 - \gamma_2)$ is the inverse of the period of the thickness oscillation. For a very thin crystal, there is an asymmetry in the thickness integrated wave-field intensity across the crystal unit cell when the g reflection is at the Bragg position, and

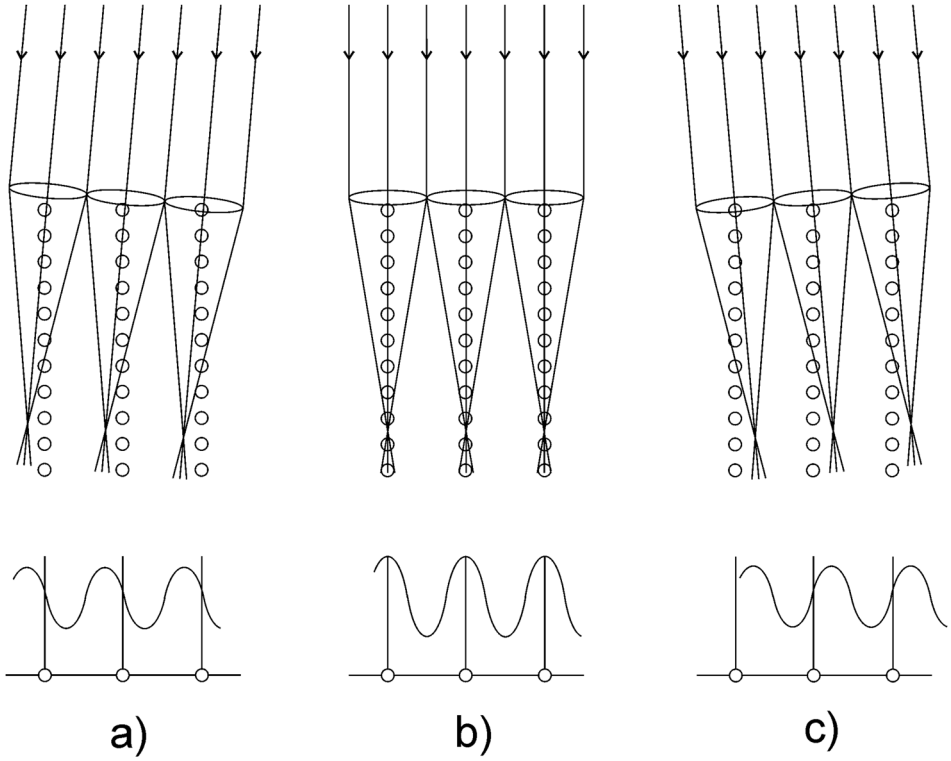

FIG. 6. An illustration, based on classical physics considerations, of how the wave field is channeled (or rather focused in the case of negative electrons) in a very thin crystal for incident electrons entering close to the crystal planes. a) and c) are slightly tilted in opposite directions and b) is parallel to the planes.

the asymmetry is inverted with the $-g$ reflection at the Bragg position.[9] Thus, the ratio between the wave-field intensities for the two-beam conditions is expected from Eq. (4) to be:

$$\frac{I_{\bar{1}\bar{1}\bar{1}}}{I_{111}} = \frac{1 - D\sin 2\pi x}{1 + D\sin 2\pi x} \tag{5}$$

where the factor D is much smaller than unity due to averaging over thickness and the diffuse scattering out of the Bragg beams (absorption). Equation (5) applies also to the 311-reciprocal lattice row by replacing 111 by 311. Figure 8 uses the experimental data of Table II. Here, Ti, Zr and Hf are considered as one entity by presenting the average of their ratios weighed by their atomic content. The curve in Fig. 8 is a guide for the eye based on adjusting the value of D (Eq. (5)) to obtain a qualitatively good fit to the observations. The origin of x (Eq. (5)) in the crystal is, for this purpose, determined by the structure factor of the 311 reflection. It is at the position giving a positive and real structure factor.[8,9] (The imaginary contribution to the structure factor is zero for this choice of origin.)

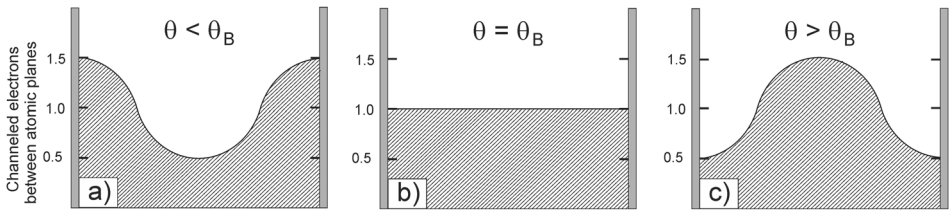

FIG. 7. Two-beam Bloch wave calculations of the thickness-averaged wave-field modulation between the atomic planes for different directions of the incident beam, a) incident beam angle smaller than the Bragg angle, b) incident beam exactly at the Bragg position and c) incident beam angle larger than the Bragg angle. While the thickness-averaged modulation is constant at the Bragg position, it varies with thickness as shown in Eq. (4).

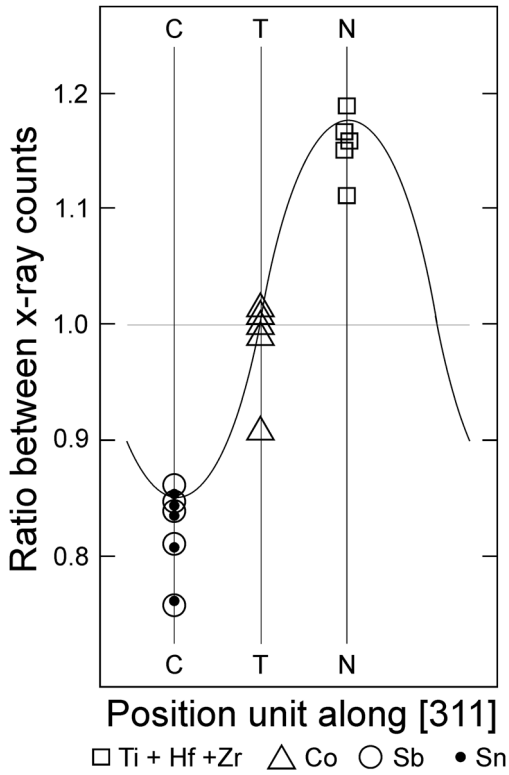

FIG. 8. Ratio between the x-ray emission counts for the five sets of measurements in Table II with the 311 and the $\bar{3}\bar{1}\bar{1}$ reflections at the Bragg position, together with estimates of the modulation based on Eq. (5) drawn as a curve.

The agreement between the estimated curve and the observations is good in Fig. 8 considering that the exact position of the origin of x is difficult to assess due to coupling with other reflections along the reciprocal row and the inaccuracies in calculating the structure factor of the 311 reflection with the many elements involved, and the compositional inhomogeneities.

The octahedral and tetrahedral atoms are exposed to different wave-field intensities when reflections along the 100-reciprocal lattice row are excited. This can be understood by considering the sequence of atomic planes in Fig. 3. Thus, the variation of the x-ray emission with incident beam direction shown in Fig. 4a and Fig. 5 is consistent with the Co atoms being on the tetrahedral sites and the other five elements on the octahedral sites. The variation in normalized x-ray emission counts with incident beam direction is much larger for Co than for the other elements. This is attributed to strong diffuse scattering of the fast electrons when the electron wave-field is confined to the plane containing the majority of atoms with high atomic number.

However, it is not possible to distinguish between C and N sites based on observations along the 200-reciprocal lattice row. For this purpose, the data shown in Table II and Fig. 8 provide further information. These observations suggest that the Ti, Zr and Hf atoms are on the N sites and Sb and Sn on the C sites The larger spread in the ratios for Hf, Zr and Ti in Table II may partly be caused by an unintentional shift in position of the electron probe on the specimen when collecting the two spectra within a pair. Thus, because of the concentration gradients caused by phase separations, the Ti, Zr and Hf contents change over small distances on the specimen (see Fig. 2); their x-ray emission counts may change more based on small position changes on the specimen than based on site preference.

An interesting observation from the SEM data in Table I is that the amount of Co tends to be slightly higher than 33 at%, around 36 at%, while the sum of Sb and Sn as well as the sum of Ti, Zr and Hf tends to be 32 at%. The excess of Co relative to the other groups of elements may suggest that some 10% of the Co atoms occupy the other tetrahedral site 4d (¾,¾,¾). However, the asymmetry across the (111) and (311) planes leaves little doubt that most of the Co atoms occupy only one of the two tetrahedral positions.

In this study, the challenges have been greater than in previous channeling studies involving oxide minerals[10] for two major reasons. The high atomic numbers of the elements cause much diffuse scattering (absorption) with the requirement of very thin crystal regions for the channeling experiments, and there are composition inhomogeneities caused by phase separation. These difficulties are compensated, to a certain degree, by the possibility of studying different reciprocal lattice rows including rows that give information about lack of centrosymmetry, and about the sense of polar axes.

The channeling technique used here is complementary to traditional crystallographic procedures based on Rietveld refinement of neutron or x-ray synchrotron data.[11] Those diffraction techniques are highly quantitative involving a large number of parameters, and their achievements are impressive considering that only one quality is directly available from the diffraction data. In the case of x-ray diffraction, this is the electron density. For that reason, however, it is difficult to provide information about atomic occupancies of elements with similar numbers of electrons, as is the case for Sn and Sb. The channeling technique used in this study is more qualitative and limited to addressing crystal site occupancies (including polarity and thus absolute position). For that purpose, the technique is robust and provides a useful supplement for crystals containing many different elements.

VI. CONCLUSION

Compositional inhomogeneity and crystal site preference have been studied for a half-Heusler material of composition $Sb_{0.8}Sn_{0.2}Ti_{0.5}Hf_{0.25}Zr_{0.25}Co$, which is a promising p-type thermoelectric material.

Spatial distribution of the elements was studied at a resolution of around 100 nm by chemical mapping through detecting the element characteristic x-ray emission using an SEM. The content of Co was relatively uniform, while the other five elements showed considerable spatial variation. Locally, the sum of the content of Sb and Sn, and the sum of the content of Ti and Zr and Hf, were nearly constant. Typically, the local content of Sb plus Sn, as well as the local content of Ti plus Zr plus Hf, was 32 at%, while the content of Co was around 36 at%.

By detecting x-ray emission under channeling conditions in a transmission electron microscope, it was found that Sb and Sn atoms occupy the 4a (0, 0, 0) position and the Ti, Zr and Hf occupy the 4b (½, ½, ½) position. The polarity observations in the channeling experiments allowed the conclusion that most of the Co atoms occupy the tetrahedral position 4c (¼, ¼, ¼). However, the higher content of Co than of the other groups of elements suggested that around 10% of the Co atoms occupy the other tetrahedral position 4d (¾, ¾, ¾).

ACKNOWLEDGMENTS

We are grateful to Dr. Wakshum Mekonnen Tucho for technical support and for financial support from the THELMA project (No. 228854).

[1] G. S. Nolas, M. Kaser, R. T. Littleton, and T. M. Tritt, Appl. Phys. Lett. **77**, 1855 (2000).
[2] J. Taftø, J. App. Cryst. **15**, 378 (1982).
[3] E. Rausch, B. Balke, S. Ouardi, and C. Felser, Phys. Chem. Chem. Phys. **16**, 25258 (2014).
[4] X. Yan, G. Joshi, W. Liu, H. Wang, S. Lee, J. W. Simonson, S. J. Poon, T. M. Tritt, G. Chen, and Z. F. Ren, Nanolett. **11**, 556 (2011).
[5] J. C. H. Spence and J. Taftø, J. Microscopy – Oxford **130**, 157 (1983).
[6] H. Geng and H. Zhang, J. Appl. Phys. **116**, 033708 (2014).
[7] G. Rogl, P. Sauerschnig, Z. Rykavets, V. V. Romaka, P. Heinrich, B. Hinterlaitner, A. Grytsiv, E. Bauer, and P. Rogl, Acta Mater. **131**, 336 (2017).
[8] J. Taftø, Micron. **34**, 157 (2003).
[9] J. Taftø, Phys. Rev. Lett. **51**, 654 (1983).
[10] J. Taftø and J. C. H. Spence, Science **218**, 49 (1982).
[11] M. N. Guzik, C. Echevarria-Bonet, M. D. Riktor, P. A. Carvalho, A. E. Gunnæs, M. H. Sørby, and B. C. Hauback, Acta Mater. **148**, 216 (2018).